Density of states of the one-dimensional electron gas: Impurity levels, impurity bands, and the band tail

A. Gold
Laboratoire de Physique des Solides, Université Paul Sabatier, 118 Route de Narbonne, 31062 Toulouse, France

A. Ghazali
Groupe de Physique des Solides, Universités Paris 6 and 7, 2 Place Jussieu, 75251 Paris, France
(Received 13 December 1993)

The density of states of cylindrical quantum wires is calculated in the presence of charged impurities located in the center of the wire. A multiple-scattering approach (Klauder's fifth approximation), which represents a self-consistent t-matrix approximation, is used. For small impurity densities and in the weak screening limit the ground-state impurity band and four excited-state impurity bands are obtained within our approach. We find good agreement between the numerically obtained spectral densities with the corresponding analytical spectral densities calculated with the single-impurity wave functions. The merging of impurity bands is studied. For large impurity densities we obtain a band tail. We present an analytical expression for the disorder-induced renormalized band-edge energy in the band-tail regime.

I. INTRODUCTION

The density of states of doped semiconductors is of considerable theoretical and experimental importance.[1] Using the multiple-scattering approach of Klauder,[2] the density of states for disordered three-[3] and two-dimensional systems, as realized in silicon–metal-oxide semiconductor structures[4] and quantum wells,[5] has been calculated. The transition from an impurity band to a band-tail regime has been discussed. It was shown that within the fifth Klauder approximation excited impurity bands can be described.[6] In this paper we study the density of states of the disordered quasi-one-dimensional electron gas confined in a cylindrical wire of radius R_0.

The behavior of electrons in quasi-one-dimensional quantum wires has been studied extensively in theory[7] and experiments[8] during the last years. Analytical results for the subband structure in cylindrical quantum wires appeared in a classical textbook on quantum mechanics.[9] Analytical results for the electron-electron interaction potential and the electron-impurity interaction potential have been derived recently[10] for cylindrical wires. We use the analytical results of that paper.

Bound-state energies in quasi-one-dimensional structures have been studied in wires with rectangular cross section and with circular cross sections.[10–27] In these calculations a single impurity is considered. The most interesting result of these calculations is the observation that the bound-state energies are strongly enhanced due to the reduced dimension. The ground-state energy for ideally two-dimensional systems[9,28] is known to be already strongly lowered to -4 Ry compared to -1 Ry for three dimensions. Finite width effects reduce the binding energy in two dimensions. While analytical results for the hydrogen atom in ideally two-dimensional systems are available,[9] we remark that analytical results for impurity levels in quasi-one-dimensional systems have not been published in the literature.

The effect of overlapping bound states due to a finite impurity density and the formation of impurity bands in one-dimensional systems has been considered in Refs. 29–31. However, within these calculations the transition from an impurity band to a band tail cannot be described. In addition, in these calculations excited impurity bands are not obtained.

In the limit of large impurity density a band-tail description for the density of states is appropriate. Theoretically, such a band tail in one-dimensional systems can also be obtained within the Born approximation[32–35] and the coherent potential approximation (CPA).[36] The self-consistent Born approximation corresponds to the third Klauder approximation. Our calculations, which are performed within the fifth Klauder approximation, are even more precise than calculations within the self-consistent Born approximation. Let us mention that some analytical results have been obtained within the Born approximation.[35] Within the commonly used CPA,[37] only the δ-function random potential can be treated. In fact, neglecting multiple occupancy corrections, the fifth Klauder approximation is equivalent to the CPA.[3] However, unlike the latter, it may include the spatial dependence of the random potential.

The purpose of this paper is twofold. First, we present a systematic analytical approach for the ground state, and for the excited states of a single hydrogenic donor located on the axis of a cylindrical wire. We study wave functions, symmetry, energy levels, and the conduction subbands involved. Our results enable us to clarify and complete an earlier work.[13] Second, it is clear that these calculations[13] are no longer valid at finite impurity concentrations, where the overlapping of wave functions cannot be neglected. To describe this situation we use a multiple-scattering approach which allows us to study numerically the impurity band in its ground state and its excited states. In the limit of low concentration, by analyzing the spectral density and the density of states,

0163-1829/94/49(23)/16480(14)/$06.00

we determine the symmetry of the excited states and the energy ordering. For large impurity concentrations a band tail is found as a result of the overlapping of conduction and impurity bands.

The paper is organized as follows. The model and the theory are described in Sec. II. Analytical results for impurity levels are presented in Sec. III. In Sec. IV we present our numerical results for impurity bands. The band-tail regime is described in Sec. V. We discuss our theory and results in Sec. VI, and conclude in Sec. VII.

II. MODEL AND THEORY

In this section we briefly discuss the model, as formulated in Ref. 10, and the theory, as formulated in Refs. 2, 3, and 5. For details we refer the reader to the original papers. Actually, the parameter space of the problem studied is large. In this paper we present results in a certain region of this space. If some experimental results appear in future publications, we shall provide additional results adapted to these experiments. The present paper provides information about general trends in quantum-wire structures, and should be useful for experimenters.

A. Model

We consider a cylindrical quantum wire[10] with the wire axis in the z direction. For a wire with radius R_0 the confining potential is given by U_c $(r \leq R_0)=0$ and U_c $(r > R_0) \rightarrow \infty$. The electron gas in the wire is characterized by the electron density N. The charged impurities are assumed to be distributed randomly on the surface of a cylinder of radius R around the wire axis, and are specified by the (one-dimensional) impurity density N_i. In this paper we study impurities located on the wire axis with $R=0$. Impurities located outside the wire with $R > R_0$ could also be studied. The electron-impurity interaction is given by $V_{11}^{ei}(\mathbf{q},R)$ for electrons in the lowest subband.[10]

Wave numbers along the wire axis are expressed in units of $1/a^*$, and $a^*=\varepsilon_L/m^*e^2$ is the effective Bohr radius with the Planck constant $h=2\pi$. m^* is the effective mass, and ε_L is the dielectric constant of the background. The energy is expressed in units of the effective Rydberg Ry* given by $\mathrm{Ry}^*=m^*e^4/2\varepsilon_L^2$. Our numerical results are given for GaAs with $m^*=0.067m_e$ and $\varepsilon_L=13$ ($a^*=103$ Å, Ry* $=5.4$ meV). m_e is the electron mass in vacuum.

Many-body effects as studied in Ref. 38 are neglected. However, we study the effect of screening where the dielectric function $\varepsilon(q,R_0,N)$ is calculated within the random-phase approximation (RPA):[39] $V_{1,s}(q)=V_{11}^{ei}(q,R)/\varepsilon(q,R_0,N)$. In fact, we always use the screened potential, and we discuss two cases. The weak screening limit ($N \ll N_i$) is characterized by a small electron density in the dielectric function ($N \sim 1\ \mathrm{cm}^{-1}$). This limit is used to study impurity levels and impurity bands. The physical idea behind this approach is the fact that in the low-density limit the charged carriers are bound to impurities and cannot contribute to the screening. For the strong screening limit we use $N=N_i$. This is the limit of quasifree electrons in which we study the band-gap renormalization.

The parameter space is given by N and R_0 for the electron gas, and by N_i and R for the impurities. In this paper we present results for $R_0=a^*$ and $R=0$. A systematic study is performed for the variables N and N_i.

B. Theory

We present numerical results within the multiple-scattering approach for the density of states of quasi-one-dimensional systems in the presence of charged impurities. Klauder's fifth approximation[2] is used for the calculation of the Green function in order to determine the density of states. The input functions in this theory are a trial Green function (e.g., the free-electron Green function), the (screened) electron-impurity interaction potential, and the electron dispersion law, which we assume to be parabolic $\varepsilon(k)=k^2/2m^*$ within a single subband.[3] For $N_i \rightarrow 0$ we use the weak screening approximation $N \ll N_i$, and for large impurity density we use the full screening properties with $N=N_i$. Disorder effects on the screening function are neglected.

The perturbed Green function $G(k,E)$ for wave vector k and energy E is given in terms of the self-energy $\Sigma(k,E)$ as

$$G(k,E)=\frac{1}{E-k^2/2m^*-\Sigma(k,E)} . \tag{1}$$

We note that $-\infty < ka^* < \infty$. The self-energy has a real part $\Sigma'(k,E)$ and an imaginary part $\Sigma''(k,E)$, and is expressed in terms of the vertex function $U(k,k,E)$ as[3]

$$\begin{aligned}\Sigma(k,E)&=\Sigma'(k,E)+i\Sigma''(k,E)\\&=\lim_{q\rightarrow k}[U(k,q,E)-N_iV_{1,s}(k-q)] .\end{aligned} \tag{2}$$

$U(k,q,E)$ is calculated in Klauder's fifth approximation as

$$\begin{aligned}U(k,q,E)&=N_iV_{1,s}(k-q)\\&\quad+\frac{1}{2\pi}\int_{-\infty}^{\infty}dq'V_{1,s}(q'-q)G(q',E)U(k,q',E) .\end{aligned} \tag{3}$$

For the quasi-one-dimensional electron gas only a one-dimensional integration appears in the nonlinear integral equation (3). This equation corresponds to Klauder's fifth approximation[2] for multiple scattering. Impurity bands and band tails can be described within this approach. Recently, it was demonstrated that excited impurity bands can be obtained within this approach.[6] For a two-dimensional electron gas, it was shown that the spectral density is described by the squared Fourier transform of the wave function of the ground and excited impurity states.

The spectral density $A(k,E)$ is given by the imaginary part of the Green function as

$$-A(k,E)=\pm\mathrm{Im}[G(k,E\pm i0]/\pi . \tag{4a}$$

$A(k,E)$ defines the density of states (DOS) as

$$\rho(E)=\frac{1}{L}\sum_{k,\sigma}A(k,E)\ . \tag{4b}$$

L is the length of the wire. The subscript σ in Eq. (4b) represents the summation over the spin states, and the DOS is given as the k integral over the spectral density. The DOS is given in units of $1/\mathrm{Ry}^*a^*$.

III. IMPURITY LEVELS

In this section we present some analytical results for a single impurity located in the center of the wire. It should be stressed that our analytical calculations presented here are not intended to give exact values for the bound-state energies. Our motivation is to obtain simple, but yet accurate, analytical expressions for the wave functions which can be Fourier transformed. In fact, as will be shown below, the Fourier-transformed wave functions can be compared with the spectral density obtained numerically within the Klauder approach, and help to identify the symmetry and the energy ordering of the bound states and to understand level mixing in the multiple-scattering approach due to a finite impurity density. We also use these analytical expressions to argue that our numerical calculations are correct, because a good agreement is found with the numerically computed spectral density in the limit of low impurity density.

A. Schrödinger equation for a single impurity

For $r\le R_0$ the Schrödinger equation of a single electron in the presence of a charged impurity located at $\mathbf{r}=(0,0,0)$ is written in cylindrical coordinates as

$$-\frac{1}{2m^*}\left[\frac{\partial^2}{\partial r^2}+\frac{1}{r}\frac{\partial}{\partial r}+\frac{1}{r^2}\frac{\partial^2}{\partial\varphi^2}+\frac{\partial^2}{\partial z^2}\right]\Phi(r,\varphi,z)-\frac{e^2}{\varepsilon_L[r^2+z^2]^{1/2}}\Phi(r,\varphi,z)=E\Phi(r,\varphi,z)\ . \tag{5a}$$

The solutions of this equation are found within the ansatz

$$\Phi(r,\varphi,z)=\phi(r)\psi(z)\exp(im\varphi)\ . \tag{5b}$$

Without the charged impurity the first subband (1SB) is characterized by $m=0$, and plane waves in the z direction: $\psi(z)\propto\exp(ikz)$. The exact solution for Eq. (5a) without impurities ($e^2=0$) was given in Ref. 9 in terms of Bessel functions. We used a simpler approach in order to calculate the averaged Coulomb interaction potential and the electron-impurity interaction potential in analytical form.[10] Therefore, in this paper we do not use the exact form for $\phi(r)$ but the approximate functions chosen in Ref. 10. The first subband is characterized by $m=0$, and $\phi(r)$ is given as $\phi_1(r)=(3/\pi R_0^2)^{1/2}[1-r^2/R_0^2]$, and the subband energy is $E_{1\mathrm{SB}}=6\ \mathrm{Ry}^*a^{*2}/R_0^2$. Averaging Eq. (5a) over r and φ with $\phi_1(r)$ results in

$$-\frac{1}{2m^*}\frac{\partial^2}{\partial z^2}\psi(z)+V_1(z)\psi(z)=(E-E_{1\mathrm{SB}})\psi(z)\ , \tag{6a}$$

with

$$V_1(z)=-\mathrm{Ry}^*\frac{32a^*}{5R_0}\{[1+(z/R_0)^2]^{5/2}-\tfrac{15}{8}|z/R_0|-\tfrac{5}{2}|z/R_0|^3-|z/R_0|^5\}\ . \tag{6b}$$

We obtain the following asymptotic behaviors: $V_1(z\to0)=-32\ \mathrm{Ry}^*a^*[1-15|z|/8R_0]/5R_0$ and $V_1(z\to\pm\infty)=-2\ \mathrm{Ry}^*a^*/|z|$. Equation (6a) represents a one-dimensional Schrödinger equation for the impurity levels attached to the lowest subband. The potential is symmetric with respect to z (see Fig. 1). Correspondingly, the eigenfunctions are either even or odd.

The second subband (2SB) is characterized by $m=\pm1$ and $\phi_2(r)=(12/\pi R_0^2)^{1/2}[r/R_0-r^3/R_0^3]$ and the subband energy is $E_{2\mathrm{SB}}=16\,\mathrm{Ry}^*a^{*2}/R_0^2$. The one-dimensional Schrödinger equation for the wave function in the z direction, by averaging over $\phi_2(r)\exp(\pm i\varphi)$, is written as Eq. (6a) with

$$V_2(z)=-24\ \mathrm{Ry}^*\frac{a^*}{R_0}\{\tfrac{16}{105}[1+(z/R_0)^2]^{5/2}[1-6(z/R_0)^2]+|z/R_0|^3[\tfrac{4}{3}+\tfrac{32}{15}(z/R_0)^2+\tfrac{32}{35}(z/R_0)^4]\}\ . \tag{7}$$

The asymptotic behaviors are given as $V_2(z\to0)=-128\ \mathrm{Ry}^*a^*[1-7z^2/2R_0^2]/35R_0$ and $V_2(z\to\pm\infty)=-2\ \mathrm{Ry}^*a^*/|z|$. $V_2(z)$ versus z is shown in Fig. 1. We mention that the first derivative of $V_1(z)$ is discontinuous at $z=0$ (see Fig. 1). The cusp in $V_1(z)$ is due to the fact that the wave function $\phi_1(r)$ at the charged center at $r=0$ is finite. For the second subband the wave function $\phi_2(r)$ at $r=0$ is zero, and the first derivative of $V_2(z)$ is continuous.

Due to $m=0$ the first subband has a degeneracy of 1. The second ($m=\pm1$) and third ($m=\pm2$) subbands have a degeneracy of 2. The fourth subband has $m=0$, and the degeneracy is again 1. The fifth, sixth, seventh, and

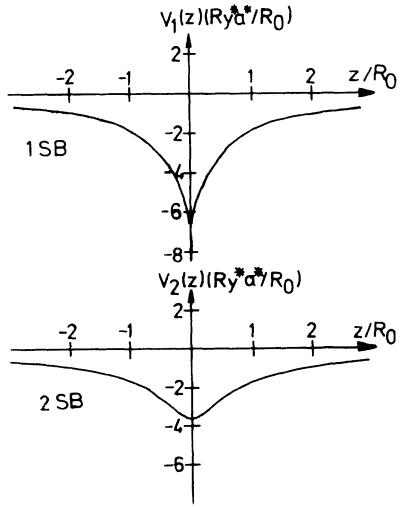

FIG. 1. $V_1(z)$ for the first subband, and $V_2(z)$ for the second subband vs z according to Eqs. (6b) and (7), respectively.

eighth subbands have again a degeneracy of 2 ($m=\pm3$, ±4, ±5, and ±6). The degeneracy of the subbands is related to the zeros of Bessel functions (see Ref. 9).

B. Variational approach for the ground state

Due to the symmetry of $V_1(z)$, we argue that the bound-state levels of each subband can be characterized by their principal quantum number and their parity. It follows that the ground state has even parity (+), and the quantum number 1. The two lowest excited states are characterized by the quantum number 2 with even (+) and odd (−) symmetries, respectively. As usual, the odd state has a lower energy than the even state. Therefore, the energy ordering of the bound states is $1^+, 2^-, 2^+, 3^-, 3^+, \ldots$.

For the ground-state energy level we use the wave function

$$\psi_{1^+}(z)=\alpha^{1/2}\exp(-\alpha|z|)=\psi_{1^+}(-z)\ , \tag{8}$$

with the variational parameter α. We find for the averaged potential, defined as $\langle V_1\rangle_{1^+1^+}=\langle\psi_{1^+}|V_1(z)|\psi_{1^+}\rangle$, the analytical expression

$$\langle V_1\rangle_{1^+1^+}=12\ \mathrm{Ry}^*\frac{a^*}{R_0^3\alpha^2}\left[\frac{2}{R_0^3\alpha^3}+\frac{1}{R_0\alpha}+\frac{R_0\alpha}{2}+\pi[Y_3(2R_0\alpha)-H_3(2R_0\alpha)]\right]\ . \tag{9}$$

$Y_3(x)$ is a Bessel function, and $\mathbf{H}_3(x)$ is a Struve function.[40] For the kinetic energy $\langle T_1\rangle_{1^+1^+}=\langle\psi_{1^+}|-\partial^2/2m^*\partial z^2|\psi_{1^+}\rangle$, we obtain $\langle T_1\rangle_{1^+1^+}=\mathrm{Ry}^*a^{*2}\alpha^2$. $\langle V_1\rangle_{1^+1^+}$ versus $2R_0\alpha$ is shown in Fig. 2, and decreases with increasing $2R_0\alpha$. In order to determine α for a given R_0, one has to find the minimum α_0 of $E_{\mathrm{var}}(\alpha)-E_{1\mathrm{SB}}=\langle T_1\rangle_{1^+1^+}+\langle V_1\rangle_{1^+1^+}$. With Eq. (9) we find $\alpha_0=0.82/a^*$ and $E_{\mathrm{var}}(\alpha_0)-E_{1\mathrm{SB}}\sim-2.73$ Ry* for $R_0=a^*$. This means that the bound state is located at -2.73 Ry* below the first conduction subband. Numerically, we find within the Klauder approach and for small impurity density $\alpha=1.12/a^*$, and $\delta E(1^+)=E(1^+)-E_{1\mathrm{SB}}\sim-2.65$ Ry* for $R_0=a^*$ (see Sec. IV). Numerical results for a single donor have been given in Ref. 13 as $\delta E(1^+)\sim-3.2$ Ry* for $R_0=a^*$. We note that in the following we take $E_{1\mathrm{SB}}=0$ and the subband edge of the free-electron gas is given by $E=0$. We conclude that the variational approach is in good agreement with the results obtained within the Klauder approach.

For $R_0\alpha\ll\frac{1}{2}$ with Eq. (9) we obtain $\langle V_1\rangle_{1^+1^+}=4\ \mathrm{Ry}^*a^*\alpha\ln(R_0\alpha)$ and $E_{\mathrm{var}}(\alpha)=\mathrm{Ry}^*a^*[a^*\alpha^2+4\alpha\ln(R_0\alpha)]$. We conclude that the variational parameter α_0 is given by $R_0=\exp[-1-a^*\alpha_0/2]/\alpha_0$, and the binding energy is expressed as $E_{\mathrm{var}}(\alpha_0)=-4\ \mathrm{Ry}^*a^*\alpha_0[1+a^*\alpha_0/4]$. These formulas become exact for $R_0/a^*\to0$ and show that the binding energy of the ground-state impurity level becomes logarithmically divergent for a small wire radius.[10] From the numerical results for $\langle V_1\rangle_{1^+1^+}$, shown in Fig. 2, we conclude that the condition $R_0\alpha_0\ll\frac{1}{2}$ is fulfilled in the limit $R_0/a^*\to0$. For $\alpha_0a^*=3$ we find $R_0/a^*=0.027$ and $E_{\mathrm{var}}(\alpha_0)=-21$ Ry*. With Eq. (9) we obtain $\alpha_0a^*=3.7$ and $E_{\mathrm{var}}(\alpha_0)=-26.6$ Ry* for $R_0/a^*=0.027$. This indicates the small range of validity of the asymptotic expression for $R_0\alpha_0\ll\frac{1}{2}$.

In Fig. 3 we show $E_{\mathrm{var}}(\alpha_0)$ and α_0 for the ground-state impurity level versus the wire radius. Our variational results are in good agreement with results obtained in the separable potential approximation,[10] and with the numerical results of Ref. 13. With decreasing wire radius the

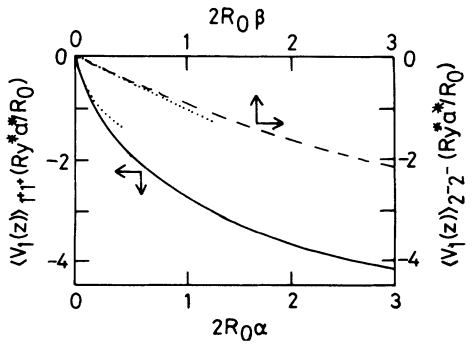

FIG. 2. $\langle V_1\rangle_{1^+1^+}$ and $\langle V_1\rangle_{2^-2^-}$ vs $2R_0\alpha$ and $2R_0\beta$ according to Eqs. (9) and (11), respectively. The dotted lines represent the analytical results for $R_0\alpha<\frac{1}{2}$ and $R_0\beta<\frac{1}{2}$.

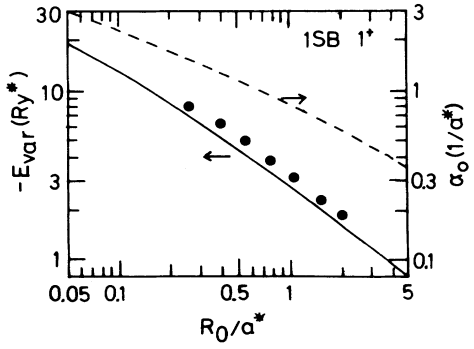

FIG. 3. Ground-state energy E_{var} (solid line) and variational parameter α_0 (dashed line) for the 1^+ state of the first subband vs wire radius R_0 according to Eq. (9). The solid dots are numerical results of Ref. 13.

binding energy increases, as has been found before.[13] Note that the numerical results[13] show a somewhat larger binding energy than our analytical results within the variational approach.

We conclude that the variational wave function underestimates the binding energy if compared with the numerical results of Ref. 13. For δ-doped GaAs, where the confining potential is similar to $V_1(z)$, a wave function as in Eq. (8) for the envelope wave function in the z direction was used.[41]

C. Impurity levels: excited bound states

For the first excited bound state we suggest the variational form

$$\psi_{2^-}(z)=(2\beta^3)^{1/2}z\exp(-\beta|z|)=-\psi_{2^-}(-z)\ . \tag{10}$$

Clearly, due to the z symmetry, $\langle\psi_{2^-}(z)|\psi_{1^+}(z)\rangle=0$. For the kinetic energy we derive $\langle T_1\rangle_{2^-2^-}=\mathrm{Ry}^*a^{*2}\beta^2$. For the potential energy $\langle V_1\rangle_{2^-2^-}=\langle\psi_{2^-}|V_1(z)|\psi_{2^-}\rangle$, we find

$$\langle V_1\rangle_{2^-2^-}=\mathrm{Ry}^*\frac{a^*}{R_0}\tfrac{16}{5}(2R_0\beta)^3\int_0^\infty dx\,x^2\exp[-2R_0\beta x](x^5+5x^3/2+15x/8-[1+x^2]^{5/2})\ . \tag{11}$$

The x integral in Eq. (11) can be calculated analytically in terms of Struve and Bessel functions. However, we found it more convenient to work with the integral form. $\langle V_1\rangle_{2^-2^-}$ versus $2R_0\beta$ is shown in Fig. 2.

For $R_0\beta\ll\frac{1}{2}$ we find $\langle V_1\rangle_{2^-2^-}=-2\ \mathrm{Ry}^*a^*\beta$ and $E_{\mathrm{var}}(\beta)=\mathrm{Ry}^*a^*\beta[a^*\beta-2]$. The minimum of $E_{\mathrm{var}}(\beta)$ is found for $\beta_0=1/a^*$. We conclude that for $R_0/a^*\to0$ for the first excited bound state $\psi_{2^-}(z)$ we obtain the energy $E_{\mathrm{var}}(\beta_0)/\mathrm{Ry}^*=-1$. This result is in agreement with the numerical calculation in Ref. 13.

With Eq. (11) and for $R_0=a^*$, we find $\beta_0=0.72/a^*$ and $E_{\mathrm{var}}(\beta_0)=-0.73\ \mathrm{Ry}^*$. Within the Klauder approach and for small impurity density, we find $\beta=0.72/a^*$ and $E(2^-)\sim-0.53\ \mathrm{Ry}^*$ for $R_0=a^*$ (see Sec. IV). $E_{\mathrm{var}}(\beta_0)$ and β_0 versus R_0 is shown in Fig. 4, together with numerical results of Ref. 13. Very good agreement is found between our variational approach and the numerical work.[13] The variation of $E_{\mathrm{var}}(\beta_0)$ with R_0 follows the variation of β_0a^* with R_0. This is a consequence of $\langle V_1\rangle_{2^-2^-}=-2\ \mathrm{Ry}^*a^*\beta[1-O(R_0\beta)]$. We mention that, contrary to the ground-state impurity level, the first-excited-state impurity level has a finite binding energy even for $R_0/a^*\to0$.

For the second excited state $\psi_{2^+}(z)$ we suggest $\psi_{2^+}(z)=\psi_{2^+}(-z)\propto[|z|+A]\exp(-\gamma|z|)$. The condition $\langle\psi_{2^+}(z)|\psi_{1^+}(z)\rangle=0$ implies that $A=-1/(\alpha+\gamma)$, and the condition $\langle\psi_{2^-}(z)|\psi_{2^+}(z)\rangle=0$ is fulfilled due to the symmetry. The corresponding expression for the kinetic energy is

$$\langle T_1\rangle_{2^+2^+}=\mathrm{Ry}^*a^{*2}\gamma^2\frac{1+4\gamma/\alpha_0+6\gamma^2/\alpha_0^2}{1+\gamma^2/\alpha_0^2}\ , \tag{12a}$$

and for the potential energy we find

$$\langle V_1\rangle_{2^+2^+}=\mathrm{Ry}^*\frac{a^*}{R_0}\tfrac{16}{5}(2R_0\gamma)^3\frac{(1+\gamma/\alpha_0)^2}{1+\gamma^2/\alpha_0^2}\int_0^\infty dx\,\exp[-2R_0\gamma x]$$
$$\times[x-1/(R_0\alpha_0+R_0\gamma)]^2(x^5+5x^3/2+15x/8-[1+x^2]^{5/2})\ . \tag{12b}$$

$\langle V_1\rangle_{2^+2^+}$ versus $2R_0\gamma$ is shown in Fig. 5 for $R_0\alpha_0=0.82$ This value for α_0 corresponds to $R_0=a^*$. Note that $\langle V_1\rangle_{2^+2^+}$ is more negative than $\langle V_1\rangle_{2^-2^-}$; however, the binding energy for the 2^+ state is smaller than for the 2^- state, as can be seen in Fig. 6.

For the 2^+ bound state, $E_{\mathrm{var}}(\gamma_0)$ and γ_0 according to Eq. (12) versus R_0 is shown in Fig. 6. For $R_0=a^*$ we find $E(2^+)\sim-0.326\ \mathrm{Ry}^*$ and $\gamma_0=0.31/a^*$. Within the multiple-scattering approach (see Sec. IV), we obtain $E(2^+)\sim-0.24\ \mathrm{Ry}^*$ and $\gamma=0.48/a^*$.

For the third excited bound state we use the odd wave function $\psi_{3^-}(z)\propto z[|z|-B]\exp(-\delta|z|)$ with the variational parameter δ. The condition $\langle\psi_{3^-}(z)|\psi_{2^-}(z)\rangle=0$ implies that $B=3/(\beta+\delta)$. We find

$$\langle T_1\rangle_{3^-3^-}=\tfrac{1}{3}\mathrm{Ry}^*a^{*2}\delta^2\frac{1-\delta/\beta_0+7\delta^2/\beta_0^2}{1-\delta/\beta_0+\delta^2/\beta_0^2}\ , \tag{13a}$$

and for the potential energy we find

TABLE I. Wave functions in the z direction $\psi_{n\pm}(z)$ and their squared Fourier transforms $|\psi_{n\pm}(k)|^2$ for $n=1$, 2, and 3.

$\psi_{n\pm}(z)$	$\lvert\psi_{n\pm}(k)\rvert^2$
$\psi_{1+}(z)\propto\exp(-\alpha\lvert z\rvert)$	$\lvert\psi_{1+}(k)\rvert^2\propto\dfrac{1}{[\alpha^2+k^2]^2}$
$\psi_{2-}(z)\propto z\exp(-\beta\lvert z\rvert)$	$\lvert\psi_{2-}(k)\rvert^2\propto\dfrac{k^2}{[\beta^2+k^2]^4}$
$\psi_{2+}(z)\propto[(\alpha+\gamma)\lvert z\rvert-1]\exp(-\gamma\lvert z\rvert)$	$\lvert\psi_{2+}(k)\rvert^2\propto\dfrac{[k^2-k_{20}^2]^2}{[\gamma^2+k^2]^4}$
$\psi_{3-}(z)\propto z[(\beta+\delta)\lvert z\rvert-3]\exp(-\delta\lvert z\rvert)$	$\lvert\psi_{3-}(k)\rvert^2\propto\dfrac{k^2[k^2-k_{30}^2]^2}{[\delta^2+k^2]^6}$
$\psi_{3+}(z)\propto[C+D\lvert z\rvert+z^2]\exp(-\eta\lvert z\rvert)$	$\lvert\psi_{3+}(k)\rvert^2\propto\dfrac{[k^4-2k_{31}^2k^2+k_{32}^4]^2}{[\eta^2+k^2]^6}$

$$\langle V_1\rangle_{3^-3^-}=\mathrm{Ry}^*\frac{a^*}{R_0}\frac{4}{15}(2R_0\delta)^5\frac{(1+\delta/\beta_0)^2}{1-\delta/\beta_0+\delta^2/\beta_0^2}\int_0^\infty dx\,x^2\exp[-2R_0\delta x]$$
$$\times[x-3/(R_0\alpha_0+R_0\gamma)]^2(x^5+5x^3/2+15x/8-[1+x^2]^{5/2})\,. \tag{13b}$$

$\langle V_1\rangle_{3^-3^-}$ versus $2R_0\delta$ is shown in Fig. 5 for $R_0\beta_0=0.72$. For the 3^- bound state $E_{\mathrm{var}}(\delta_0)$ and δ_0, which minimizes $E_{\mathrm{var}}(\delta)$, versus R_0 are shown in Fig. 6. For $R_0=a^*$ we find $E(3^-)\sim-0.156$ Ry* and $\delta_0=0.25/a^*$. Within the multiple-scattering approach we obtain (see Sec. IV), $E(3^-)\sim-0.08$ Ry* and $\delta=0.34/a^*$.

The fourth excited bound state is characterized by $\psi_{3+}(z)\propto[z^2+C|z|+D]\exp(-\eta|z|)$ with the variational parameter η. With the conditions $\langle\psi_{3+}(z)|\psi_{1+}(z)\rangle=\langle\psi_{3+}(z)|\psi_{2+}(z)\rangle=0$, the coefficients C and D are determined. The results for the wave function $\psi_{n\pm}(z)$ for $n=1$–3 are summarized in Table I.

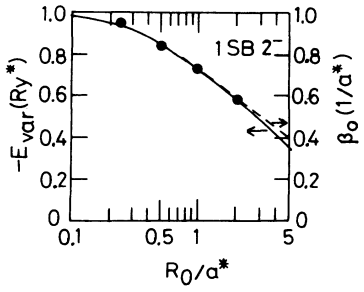

FIG. 4. Excited-state energy E_{var} (solid line) and variational parameter β_0 (dashed line) for the 2^- state of the first subband vs wire radius R_0 according to Eq. (11). The solid dots are numerical results of Ref. 13.

D. Impurity levels: second subband

The preceding results for the binding energy have been derived for the first subband. Similar calculations can be made for the second subband by using $V_2(z)$ instead of $V_1(z)$. We do not give the explicit expressions for $\langle V_2\rangle_{1^+1^+}$, $\langle V_2\rangle_{2^-2^-}$, $\langle V_2\rangle_{2^+2^+}$, and $\langle V_2\rangle_{3^-3^-}$ in this paper. However, we mention that $\langle T_2\rangle_{1^+1^+}=\langle T_1\rangle_{1^+1^+}$, $\langle T_2\rangle_{2^-2^-}=\langle T_1\rangle_{2^-2^-}$, $\langle T_2\rangle_{2^+2^+}=\langle T_1\rangle_{2^+2^+}$, and $\langle T_2\rangle_{3^-3^-}=\langle T_1\rangle_{3^-3^-}$.

Numerical results for binding energies of the 1^+ state, the $2^\pm$ states, and the 3^- state of the second subband versus R_0 are given in Fig. 7. The binding energies for the second subband are somewhat lower ($<10\%$) than for the first subband, as already noted in Refs. 10 and 13. For the excited states with $n>3$ and which are not very

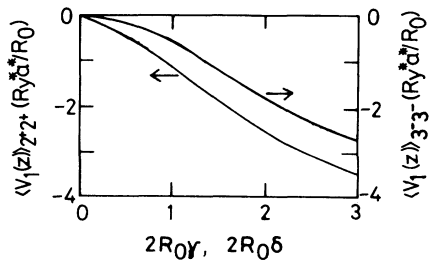

FIG. 5. $\langle V_1\rangle_{2^+2^+}$ according to Eq. (12b) with $\alpha_0=0.82/a^*$ vs $2R_0\gamma$ and $\langle V_1\rangle_{3^-3^-}$ according to Eq. (13b) with $\beta_0=0.72/a^*$ vs $2R_0\delta$ for the first subband.

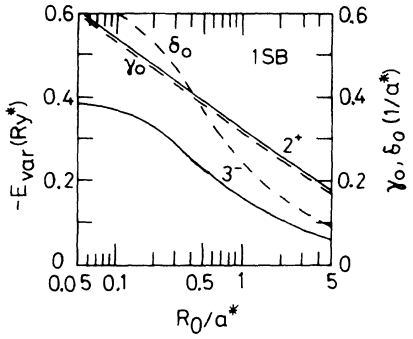

FIG. 6. Excited-state energies E_{var} for the 2^+ state $[E_{var}(\gamma_0)]$ and the 3^- state $[E_{var}(\delta_0)]$ (solid lines), and variational parameters γ_0 and δ_0 (dashed lines) vs wire radius R_0 for the first subband according to Eqs. (12) and (13), respectively.

localized in the z direction, the binding energies for the two subbands become numerically very similar. This comes from the fact that $V_1(z \gg R_0)=V_2(z \gg R_0)=-2$ Ry*$a^*/|z|$.

E. Fourier-transformed wave functions

An investigation of the squared Fourier transform of the eigenfunctions is useful not only to analyze the spectral density, but also to investigate the general behavior of the hydrogen system is connection with our variational approach.

The Fourier transform of $\psi_{1^+}(z)$ is given as $\psi_{1^+}(k)$, and we get

$$|\psi_{1^+}(k)|^2=\frac{2}{\pi}\frac{\alpha^3}{[\alpha^2+k^2]^2} . \tag{14}$$

The half width of $|\psi_{1^+}(k)|^2$ is given by

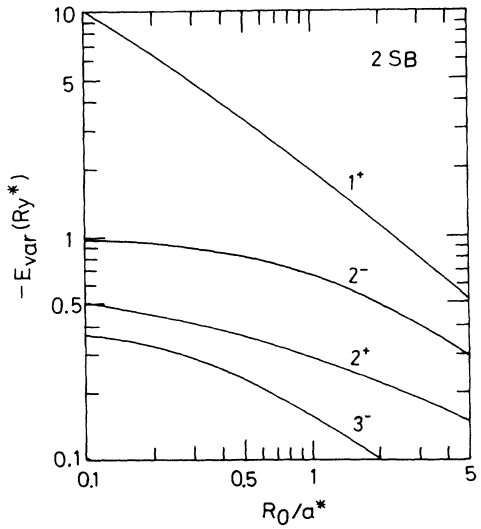

FIG. 7. Second subband: binding energy E_{var} vs wire radius R_0 for the ground-state impurity level 1^+ $[E_{var}(\alpha_0)]$ and the excited-state impurity levels 2^- $[E_{var}(\beta_0)]$, 2^+ $[E_{var}(\gamma_0)]$, and 3^- $[E_{var}(\delta_0)]$.

$k_{1/2}=\alpha[2^{1/2}-1]^{1/2}=0.643\alpha$. For large wave numbers we find $|\psi_{1^+}(k\to\infty)|^2 \propto 1/k^4$ for the ground state. For the two- and three-dimensional hydrogen atom, for the ground state one obtains $|\psi_{1s}(k)|^2 \propto 1/[1+a^{*2}k^2/4]^3$ ($E_{1s}=-4$ Ry*) with $|\psi_{1s}(k\to\infty)|^2 \propto 1/k^6$ and $|\psi_{1s}(k)|^2 \propto 1/[1+a^{*2}k^2]^4$ ($E_{1s}=-1$ Ry*) with $|\psi_{1s}(k\to\infty)|^2 \propto 1/k^8$, respectively.[9] For large wave numbers, this suggests the following dependence on the dimension d: $|\psi_{1s}(k\to\infty)|^2 \propto 1/k^{2(1+d)}$.

For $\psi_{2^-}(z)$ we obtain $|\psi_{2^-}(k)|^2=16\beta^5k^2/\pi[\beta^2+k^2]^4$. We find the following limiting behavior: $|\psi_{2^-}(k\to0)|^2 \propto k^2$ for small wave numbers and $|\psi_{2^-}(k\to\infty)|^2 \propto 1/k^6$ for large wave numbers. The maximum of $|\psi_{2^-}(k)|^2$ is at $k_{2m}=\beta/3^{1/2}=0.577\beta$. For the $\psi_{2^+}(z)$ bound state (see Table I) we find $|\psi_{2^+}(k_{20})|^2=0$ at $k_{20}=\gamma/(1+2\gamma/\alpha)^{1/2}$ and $|\psi_{2^+}(k\to\infty)|^2 \propto 1/k^4$. Similar results can be obtained for the excited bound states 3^- and 3^+; see Table I. We obtain $|\psi_{3^-}(k_{30})|^2=0$ at $k_{30}=(3\beta\delta/[4(1+\beta/4\delta)])^{1/2}$. We mention that $|\psi_{3^-}(k\to0)|^2 \propto k^2$ and $|\psi_{3^-}(k\to\infty)|^2 \propto 1/k^6$. The excited bound state 3^+ is characterized by $|\psi_{3^+}(k_{3\pm})|^2=0$ at $k_{3\pm}=[k_{31}^2\pm(k_{31}^4-k_{32}^4)^{1/2}]^{1/2}$. k_{31} and k_{32} are given, via the orthogonality condition with the states 1^+ and 2^+, in terms of α, γ, and η. We obtain $|\psi_{3^+}(k\to0)|^2 \propto k^0$ and $|\psi_{3^+}(k\to\infty)|^2 \propto 1/k^4$.

F. Wave functions: general behavior

The general expression for the bound-state wave functions (see Table I) is $\psi_{n\pm}(z) \propto P_{n-1,\pm}(z)\exp(-|z|/\alpha_{n\pm})$, where $P_{n-1,\pm}(z)$ is a polynomial of order $n-1$ in the variable z, even for the $(+)$ state and odd for the $(-)$ state. $\alpha_{n\pm}$ is found to be of order na^* (see Sec. IV B). In our system the number of nodes is determined by the zeros of $P_{n-1,\pm}(z)$.

The general behavior for the excited states in the hydrogen atom in d dimensions is $|\psi_{n1}(k\to\infty)|^2 \propto 1/k^{2+2d+2l}$ with $l=0,1,2 \le n-1$.[9] If we identify $l=0$ (s states) with $(+)$, namely 1^+, 2^+, $3^+\ldots$, and $l=1$ (p states) with $(-)$, namely 2^-, $3^-,\ldots$, this behavior also holds for the quasi-one-dimensional hydrogen atom (see Table I). From this dimensional analysis of the Fourier-transformed wave function we conclude that the variational form of the wave function is a good approximation to the exact solution. However, while the hydrogen atom in three and two dimensions can be solved analytically, this is not the case for quasi-one-dimensional cylindrical wires. Therefore, we believe that our simple variational approach is of interest not only for the spectral density analysis, as will be discussed in Sec. IV, but also for some general aspects of the hydrogen atom in d dimensions.

IV. IMPURITY BANDS

In this section we present our results for the density of states of the impurity bands in the weak screening limit $N \ll N_i$ and in the full screening limit $N=N_i$. We study the DOS, the spectral density, and screening effects.

A. Weak screening: density of states

The DOS versus energy for $N_i=1\times10^3$ cm^{-1}, $N=1\times10^0$ cm^{-1}, $R_0=a^*$, and $R=0$ is shown in Fig. 8. We found not only the ground-state impurity band (1^+) (see inset in Fig. 8), but also the first four excited-state impurity bands ($2^-,2^+,3^-,3^+$). The energy ordering for ($1^+,2^-,2^+,3^-,3^+$) is in perfect agreement with theoretical results of a variational calculation for a single impurity,[13] and with our general discussion in Sec. III.

In our calculation the five bound states are characterized by their mean energies $E(1^+)=-2.65$, $E(2^-)=-0.53$, $E(2^+)=-0.24$, $E(3^-)=-0.08$, and $E(3^+)=-0.04$ Ry*; see Fig. 8. Within a variational calculation for a single impurity,[13] the values -3.2 Ry* (1^+) and -0.75 Ry* (2^-) have been reported. Our results for the binding energies within the Klauder approach are about 20% smaller than the variational results reported in Ref. 13. This discrepancy is presumably due to the use of a finite impurity density and a finite screening effect in our multiple-scattering calculations. Indeed, both effects tend to lower the binding energy. However, in two-dimensional systems we found very good agreement[5] between the impurity energy levels in the multiple-scattering approach and the variational results.[42]

In two-dimensional systems we found numerically three impurity bands in the weak screening limit.[6] Five impurity bands have been identified for the quasi-one-dimensional system; see Fig. 8. The origin of this larger resolution is presumably the fact that in one-dimensional systems the distance between the energy levels is larger than in two- and three-dimensional systems. In three dimensions[3] the weak screening limit ($N\to0$) has not yet been studied, and no separate excited-state impurity band has yet been identified.

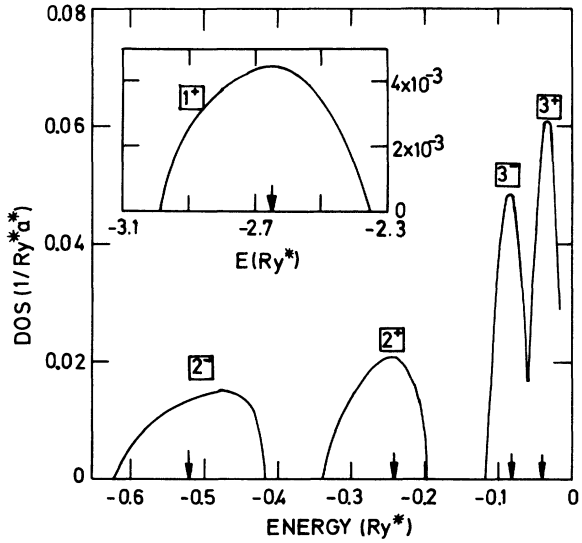

FIG. 8. Density of states (DOS) vs energy for $R_0=a^*$, $R=0$, $N_i=1\times10^3$ cm^{-1}, and $N=1\times10^0$ cm^{-1} (weak screening) in the regime of the impurity band with the ground state 1^+ (inset) and the excited impurity bands 2^-, 2^+, 3^-, and 3^+. The arrows indicate the bound-state energies for $N_i\to0$.

B. Weak screening: spectral density

In the low-density limit the spectral density is given by[6]

$$A(k,E)=\frac{1}{L}\left\langle \sum_i |\psi_i(k)|^2\delta(E-E_i)\right\rangle . \tag{15}$$

$\langle\cdots\rangle$ represents the impurity configuration average, and the sum over i runs over the eigenstates. L is the length of the wire with $L\to\infty$. We have studied the spectral density $A(k,E)$ vs the wave number. The results for certain energies are shown in Fig. 9 for $N_i=1\times10^3$ cm^{-1}, $R_0=a^*$, and $R=0$ as solid dots. The energies chosen correspond to the center of the various impurity bands. The maximum of the spectral density has been normalized to 1. $|\psi_{n\pm}(k)|^2$ according to Table I versus k is shown in Fig. 9 as the solid lines for $n=1$, 2, and 3. Their absolute maximum has been normalized to 1 in order to compare $|\psi_{n\pm}(k)|^2$ with the spectral density. For

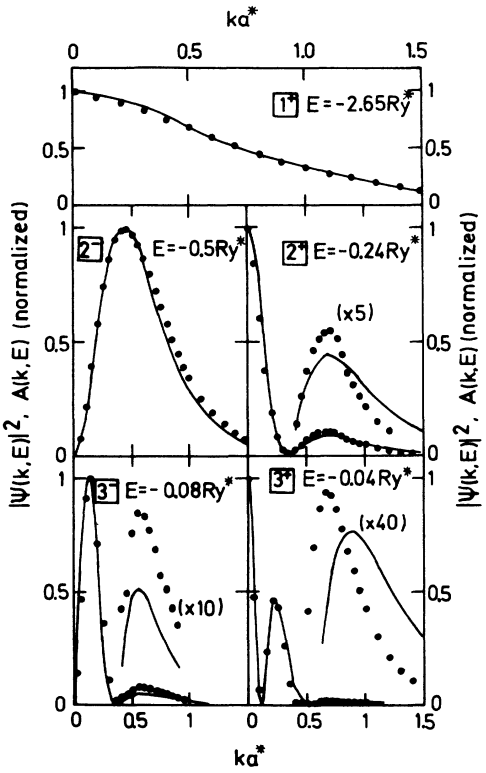

FIG. 9. Variational wave function $|\psi_{n\pm}(k)|^2$ according to Table I vs wave number k as solid lines. Numerically calculated spectral density $A(k,E)$ vs wave number for $R_0=a^*$, $R=0$, $N_i=1\times10^3$ cm^{-1}, and $N=1\times10^0$ cm^{-1} (weak screening) for the ground-state impurity band 1^+ and the excited-state impurity bands 2^-, 2^+, 3^-, and 3^+ as solid dots. The variational parameters are $\alpha=1.12/a^*$, $\beta=0.75/a^*$, $\gamma=0.48/a^*$, $\delta=0.34/a^*$, and $\eta=0.32/a^*$ with $k_{1/2}=0.72/a^*$, $k_{2m}=0.43/a^*$, $k_{20}=0.35/a^*$, $k_{30}=0.35/a^*$, $k_{31}=0.40/a^*$, and $k_{32}=0.36/a^*$.

two-dimensional systems such as analysis has already been performed in the limit of low impurity density.[6]

The parameters α, β, γ, δ, and η for $|\psi_{n^\pm}(k)|^2$ in Fig. 9 are determined by a fit to the numerical results for the spectral density for certain wave numbers. For the ground-state impurity band 1^+ we used the half-width of the spectral density: $k_{1/2}a^*=0.72$; see Fig. 9. With $k_{1/2}=0.64\alpha$, we obtain $\alpha=1.12/a^*$. The spectral density of the 2^- impurity band has a (numerically determined) maximum at $k_{2m}a^*=0.43$. Applying $k_{2m}=0.58\beta$ we derive $\beta=0.75/a^*$. For the 2^+ impurity band we find numerically $k_{20}a^*=0.35$. With $\gamma=k_{20}^2[1+(1+\alpha^2/k_{20}^2)^{1/2}]/\alpha$, we obtain $\gamma=0.48/a^*$. The 3^- impurity band has a vanishing spectral density for $k_{30}a^*=0.35$. With $\delta=2k_{30}^2[1+(1+3\beta^2/4k_{30}^2)^{1/2}]/3\beta$, we derive $\delta=0.34/a^*$. For the 3^+ impurity band we get $k_{31}=[(k_{3^-}^2+k_{3^+}^2)/2]^{1/2}$ and $k_{32}=(2k_{3^-}k_{3^+})^{1/2}$. With $k_{3^-}=0.12/a^*$ and $k_{3^+}=0.55/a^*$ from our numerical results for the spectral density, we find with $\eta=0.32/a^*$ the best fit of $|\psi_{3^+}(k)|^2$ to the spectral density.

The coefficients $1/\alpha=0.89a^*$, $1/\beta=1.33a^*$, $1/\gamma=2.08a^*$, $1/\delta=2.94a^*$, and $1/\eta=3.12a^*$ describe the extension of the wave function in the z direction. We conclude that the extension increases with increasing quantum number n. This is consistent with the energy ordering of the impurity bands found numerically; see Fig. 8.

The good agreement found between the spectral density and the squared Fourier-transformed wave functions (see Fig. 9) confirms the symmetry of the states and their energy ordering. Our results for the ground-state impurity band agree quantitatively. For higher quantum numbers $n>2$ small deviations are seen for larger wave numbers. This is expected because our analytical results for the wave functions are not exact. Nevertheless, the good agreement is very important because it gives strong evidence that our computational routine is correct.

C. Weak screening: width of the impurity band

The DOS for $R_0=a^*$ and $R=0$ versus energy is shown in Fig. 10 for different values of the impurity concentration $N_i=1\times10^4$ cm^{-1}, $N_i=5\times10^4$ cm^{-1}, $N_i=1\times10^5$ cm^{-1}, and for weak screening $N=1\times10^3$ cm$^{-1}\ll N_i$. At such impurity densities the excited impurity bands have very small binding energies and(or) have already merged with the conduction band. Let us mention that at the lowest impurity densities the DOS for $E>0$ tends to follow the $1/E^{1/2}$ law for the free-electron gas.

With increasing impurity concentration the width of the impurity band increases, and for $N_i=1\times10^5$ cm^{-1} the impurity band overlaps with the conduction subband. The computed impurity band width Γ_{1^+} is about 1.5 Ry* for $N_i=1\times10^4$ cm^{-1}, and about 3.2 Ry* for $N_i=5\times10^4$ cm^{-1}. It follows approximately the $N_i^{1/2}$ law for impurity bands expected from the CPA,[37] namely

$$\Gamma_{n^\pm}(N)=\Gamma_0(N,n^\pm)[N_ia^*]^{1/2}\ , \tag{16}$$

with $\Gamma_0(N,1^+)=15$ Ry* and $a^*=103$ Å. In the general case for arbitrary wire radius and impurity position, the prefactor $\Gamma_0(N,n^\pm)$ in Eq. (16) has to be replaced by a function $\Gamma_0(R_0,R,N,n^\pm)$. We expect that $\Gamma_0(R_0,R,N,n^\pm)$ decreases with increasing R_0 and increasing R.

For $N_i=1\times10^5$ cm^{-1} we obtain according to Eq. (16), $\Gamma_{1^+}/\text{Ry}^*=1.5\times10^{1/2}=4.7$, which is roughly the numerical value; see Fig. 10. Note that the binding energy of the center of the impurity band $E_{1^+}=-2.0$ Ry* is smaller than in Fig. 8, where $E_{1^+}=-2.65$ Ry*. This shift is due to the larger electron density $N=1\times10^3$ cm^{-1} used for Fig. 10 (more screening). If $N_i\sim1\times10^5$ cm^{-1} corresponds to the critical density N_{ic} of the merging between the impurity band and the conduction band, we conclude that

$$N_{ic,n^\pm}a^*=f(N,n^\pm)\ , \tag{17}$$

with $f(N=1\times10^3\text{ cm}^{-1},1^+)=0.1$. This value is smaller than the Mott density for three-dimensional systems $N_{ic}^{1/3}a^*=0.25$,[43] if the $N_{ic}^{1/d}$ scaling law is used. For quantum wells of width $L=a^*$ and $3a^*$ with impurities in the center of the well, we found $N_{ic}^{1/2}a^*=0.28$ and 0.1, respectively.[5] In fact, we expect that in general $N_{ic,n^\pm}a^*=f(R_0,R,N,n^\pm)$, and that $f(R_0,R,N,n^\pm)$ decreases with increasing R_0 and increasing R.

A systematic study of the band-edge energies versus the impurity concentration is performed in Fig. 11 for $N=1\times10^0$ cm^{-1}, where excited impurity bands are also investigated. The dashed lines in Fig. 11 indicated a minimum in the DOS, while the solid lines indicate a vanishing DOS. The impurity bands for the $3^\pm$ levels are only shown in the upper part of Fig. 11, where an enlarged energy scale is used. For the 1^+-state impurity band we find $\Gamma_{1^+}(N=1/\text{cm})=20$ Ry*$[N_ia^*]^{1/2}$ [see Eq.

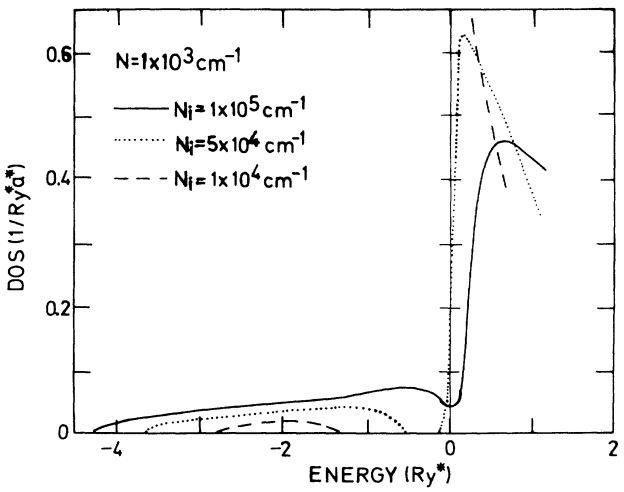

FIG. 10. Density of states (DOS) vs energy for $R_0=a^*$, $R=0$, and different impurity densities $N_i=1\times10^4$ cm^{-1}, $N_i=5\times10^4$ cm^{-1}, and $N_i=1\times10^5$ cm^{-1}. The weak screening approximation with $N=1\times10^3$ cm^{-1} ($N\ll N_i$) is used.

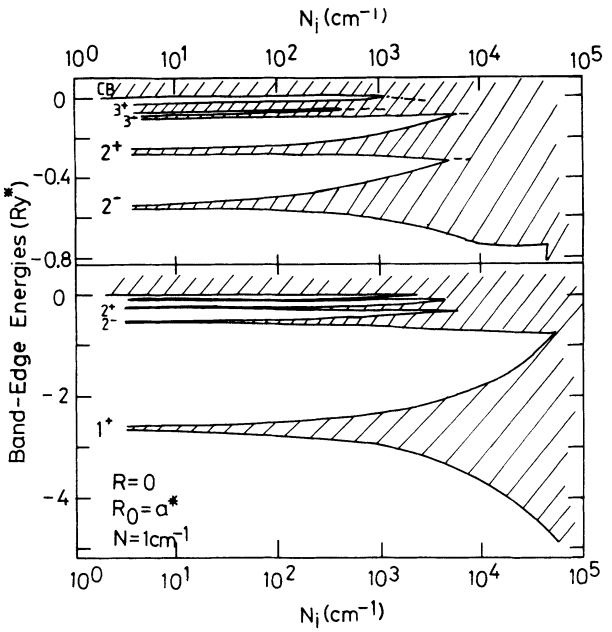

FIG. 11. Band-edge energies of the impurity bands for the 1^+ impurity level, the $2^{\pm}$ impurity levels, and the $3^{\pm}$ impurity levels vs impurity density N_i for $R_0=a^*$, $R=0$, and $N=1\times10^0$ cm^{-1}. The excited impurity bands are shown in the upper part with an enlarged energy scale. The dashed lines indicate a minimum in the DOS, and the dashed-dotted line a shoulder in the DOS. The conduction band is indicated by CB. The ground-state impurity band is shown in the lower part of the figure.

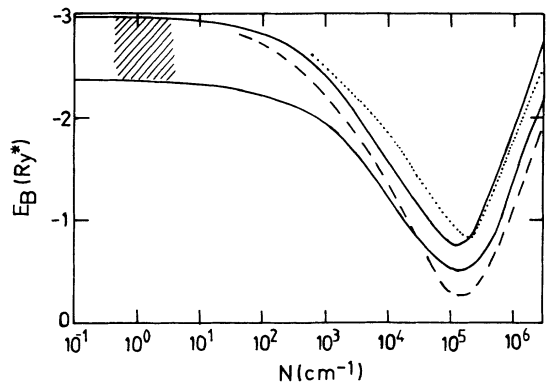

FIG. 12. Ground-state impurity band energy vs density N for $R_0=a^*$, $R=0$, and $N_i=1\times10^3$ cm^{-1}. The solid lines correspond to the band edges calculated in the fifth Klauder approximation. The hatched area describes the width of the impurity band. The dashed and dotted lines are theoretical results for a single impurity from Refs. 10 and 17, respectively.

(16)], and $\Gamma_{1^+}(N=1/\text{cm})/|E_{1^+}|=7.5[N_i a^*]^{1/2}$. For the 2^--state impurity band we obtain $\Gamma_{2^-}(N=1/\text{cm})=6.5$ $\text{Ry}^*[N_i a^*]^{1/2}$ and $\Gamma_{2^-}(N=1/\text{cm})/|E_{2^-}|=12.3$ $[N_i a^*]^{1/2}$. This indicates that ratio $\Gamma_{n^{\pm}}/|E_{n^{\pm}}|$ increases with increasing quantum number n.

The merging of the 1^+ impurity band with the 2^- impurity band occurs (see Fig. 11) at $N_{ic,1^+}=5\times10^4$ cm^{-1}: $f(N=1/\text{cm},1^+)=0.05$; see Eq. (17). The merging of the 2^- impurity band with the 2^+ impurity band occurs at $N_{ic,2^-}=5\times10^3$ cm^{-1}; $f(N=1/\text{cm},2^-)=0.005$. Due to the increasing extension of the wave functions with increasing quantum number n, the critical density $N_{ic,n^{\pm}}$ for the merging decreases with increasing quantum number; see Fig. 11. From our numerical results summarized in Fig. 11 we conclude that $f(R_0,R,N,n^{\pm})/|E_{n^{\pm}}(R_0,R)|$ also depends on the quantum number, and decreases with increasing quantum number. Let us mention that in two-dimensional systems for the ground-state impurity band we found that the ratios $N_{ic,1}(z_i)/E_1(z_i)$ are nearly independent of the impurity position z_i.[5]

We have also studied the spectral density versus the impurity concentration, and the results obtained for quasi-one-dimensional wires are similar to the results obtained for two-dimensional systems.[6] Therefore, we do not report explicit results in this paper.

D. Screening effect for the binding energy

We have calculated the impurity band for the ground state versus electron density for $N_i=1\times10^3$ cm^{-1}, $R_0=a^*$, and $R=0$. Our results are shown in Fig. 12. With increasing density the energy of the impurity band decreases due to screening. However, we notice that for $N>1\times10^5$ cm^{-1} the energy increases again with increasing density, and we find a well-pronounced minimum around $N\sim1\times10^5$ cm^{-1}. This effect is already known for a single impurity, and the results of these calculations are shown in Fig. 12 as dashed[10] and dotted[17] lines. We mention that this behavior is a peculiar effect due to the quasi-one-dimensional structure studied in this paper. In three dimensions the binding energy of the ground state decreases with increasing density and vanishes at a certain electron density (the Mott value[43]). In two dimensions the binding energy depends on the well width and becomes constant for large electron density.[44] The increase of the binding energy at large electron densities is a consequence of the structure of the dielectric response in one-dimensional systems, which reflects the effect of the confinement.

It is interesting to note that for $N<1\times10^4$ cm^{-1} the bandwidth decreases with decreasing binding energy (increasing density), while for $N>1\times10^4$ cm^{-1} the bandwidth is unchanged when the binding energy increases by a factor 5 between 1×10^5 $cm^{-1}<N<1\times10^7$ cm^{-1}.

V. BAND TAILS

In this section we present results for large impurity densities. In this density range the various impurity bands have already merged with the conduction band, and the DOS is described as a band tail. However, the study of the spectral density clearly indicates that disorder effects are still very important.

A. Density of states and spectral density

For large impurity concentrations a band tail in the DOS is obtained. A representative result for $N_i=N=1\times10^6$ cm^{-1}, $R_0=a^*$, and $R=0$ is shown in Fig. 13. The density of states of the one-dimensional free-electron gas is written as $\rho^{(0)}(E)=(1/\mathrm{Ry}^*a^*)(\mathrm{Ry}^*E)^{1/2}/\pi$. The $\rho^{(0)}(E)\propto 1/E^{1/2}$ singularity for energy $E\to0$ is destroyed by disorder. States near $E\sim0$ are shifted to negative energies, and this gives rise to states in the band gap. The energy range ε_c of this disorder-induced band-gap renormalization is shown in Fig. 13. The Fermi energy ε_F is weakly shifted by disorder effects; see Fig. 13. We note that the density of states at the Fermi energy is slightly reduced by disorder, $\rho(\varepsilon_F)<\rho^{(0)}(\varepsilon_F^{(0)})$, but the slopes of the DOS around ε_F and $\varepsilon_F^{(0)}$ are very different.

The spectral density $A(k,\varepsilon_F)$ for $N_i=N=1\times10^6$ cm^{-1}, $R_0=a^*$, and $R=0$ is shown in Fig. 14. For the electron gas without disorder the spectral density $A(k,E)\propto\delta(E-k^2/2m^*)$ is described by a δ peak at $k=(2m^*E)^{1/2}$. It is evident that disorder effects are very strong, as seen in Fig. 14: they result in a broad spectral density with a smooth peak shifted toward $k=0$. Without disorder the δ peak of the spectral density in Fig. 14 is at $k_F=1.84/a^*$.

The real part $\Sigma'(k,\varepsilon_F)$ and the imaginary part $\Sigma''(k,\varepsilon_F)$ of the self-energy at the Fermi energy $\varepsilon_F=3.4$ Ry* versus the wave number are shown in Fig. 15 for the same parameters as used in Fig. 14: $N_i=N=1\times10^6$ cm^{-1}, $R_0=a^*$, and $R=0$. We note that for $ka^*<1$ the self-energy components at the Fermi energy are of the same order as the Fermi energy; $\Sigma'(k=0,\varepsilon_F)=2.3$ Ry* and $\Sigma''(k=0,\varepsilon_F)=2.0$ Ry*. For large wave numbers the self-energy becomes small. At the Fermi wave number $k_F=1.84/a^*$, we find $\Sigma'(k_F,\varepsilon_F)=0.29\varepsilon_F$ and $\Sigma''(k_F,\varepsilon_F)=0.85\varepsilon_F$. This indicates that disorder effects

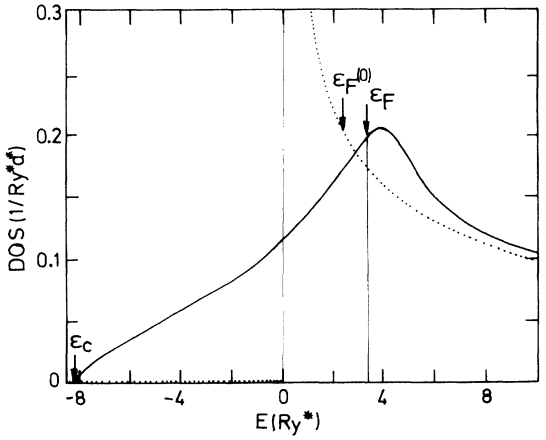

FIG. 13. Density of states (DOS) vs energy E as solid line for $R_0=a^*$, $R=0$, $N_i=1\times10^6$ cm^{-1}, and $N=N_i$ (full screening). The dotted line represents the DOS of the free-electron gas. ε_c describes the band-tail energy edge induced by disorder. The Fermi energy ε_F of the disordered electron gas and the Fermi energy $\varepsilon_F^{(0)}$ of the free-electron gas are indicated.

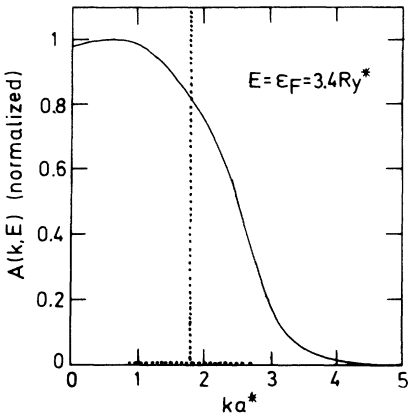

FIG. 14. Spectral density $A(k,\varepsilon_F)$ at the Fermi energy ε_F vs wave number k for $R_0=a^*$, $R=0$, and $N_i=N=1\times10^6$ cm^{-1} (same values as in Fig. 13) as solid line. The dotted line is the δ peak for the free-electron gas at $k=(2m^*\varepsilon_F^{(0)})^{1/2}$.

are very important for an understanding of the spectral density and the DOS in quasi-one-dimensional systems. We note that both $\Sigma'(k,\varepsilon_F)$ and $\Sigma''(k,\varepsilon_F)$ are strongly dependent on the wave number up to $ka^*=5$. This result reflects the long-range random potential (Coulomb potential). This contrasts with the tight-binding CPA, where the self-energy is independent of k.

B. Band-gap renormalization

In Fig. 13 we have indicated the band-tail edge ε_c. The energy ε_c measures the reduction of the band gap due to the conduction-band lowering by disorder. A systematic study of ε_c versus $N=N_i$ is shown in Fig. 16 for $R_0=a^*$ and $R=0$. Our numerical results are well described by

$$\varepsilon_c=-8.0\ \mathrm{Ry}^*[N/10^6\,\mathrm{cm}^{-1}]^{0.8}\ . \tag{18}$$

Equation (18) is represented by the solid line in Fig. 16. We mention that the prefactor in Eq. (18) will depend on the position of the impurities R, and will decrease for im-

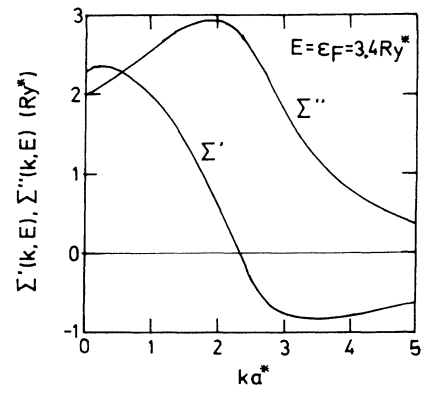

FIG. 15. Self-energy components $\Sigma'(k,\varepsilon_F)$ and $\Sigma''(k,\varepsilon_F)$ at the Fermi energy ε_F vs wave number k for $R_0=a^*$, $R=0$, and $N_i=N=1\times10^6$ cm^{-1}.

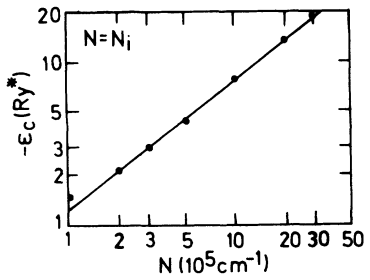

FIG. 16. Renormalization energy ε_c of the conduction-band edge for $R_0=a^*$, $R=0$, and $N=N_i$ vs electron density N as solid dots. The solid line represents Eq. (18).

purities located outside the axis of the wire. For increasing wire radius the prefactor in Eq. (18) will decrease.

We conclude that disorder produces a very large band tail in quasi-one-dimensional systems when compared with two-[5] or three-dimensional[3] electron gases. For example, for GaAs quantum wells of width $L=a^*$ with impurities in the center of the well, we found[5] $\varepsilon_c=-1.3$ Ry* $[N/10^{11}\ \text{cm}^{-1}]^{0.5}$. For three-dimensional systems the behavior $\varepsilon_c \propto -N^{1/3}$ was found.[3] In general, one expects $\varepsilon_c \propto -N^{\nu}$ with $\nu=1/d$. d is the dimension of the system. Our value $\nu=0.8$ for wires [see Eq. (18)] is smaller than expected due to the finite cross section.

VI. DISCUSSION

In this section we discuss our theory and results. Some comparison with existing theories is made. It will become clear that our theory is semiquantitative. However, the qualitative aspects of the theory are correct. We shall discuss some peculiar features of the quasi-one-dimensional system studied in this paper.

A. Model and theory

In our calculation we used an infinite barrier confinement. In real structures the barrier height is finite, and the wave function will penetrate into the barrier. This gives rise to a reduction of the bound-state energies, as has already been discussed in various publications. Our one-subband approximation implies that the Fermi energy is smaller than the intersubband energy $E_{2SB}-E_{1SB}=10$ Ry*$(a^*/R_0)^2$. With $N^2a^{*2}=4\varepsilon_F/\pi^2$ Ry* and $R_0=a^*$, the condition for the Fermi energy is $\varepsilon_F<10$ Ry*, and for GaAs the electron density must be smaller than $N=2.0\times10^6\ \text{cm}^{-1}$.

We used two approximations for the screening. For small impurity density we applied the random-phase approximation (RPA) in the week screening limit where $N\ll N_i$. Within this approach we considered the electrons as localized. For large impurity density we applied the RPA in the strong screening limit where $N=N_i$. Clearly, this approach corresponds to nonlocalized electrons. Theoretically, it is well known that one-dimensional systems are always localized in the limit of vanishing temperature.[45] However, the latter result was derived for a short-range random potential and noninteracting electrons. Experimentally, the transport properties of quasi-one-dimensional systems are presently under study, and it seems that the conductivity can be quite large. Shubnikov–de Haas oscillations and a finite conductivity have been observed in experiments with quasi-one-dimensional systems. Therefore, we think that our two approaches for the screening are justified.

Our calculations are performed in the fifth Klauder approximation which corresponds to a self-consistent t-matrix approximation. Multiple-occupancy corrections, which become important at large impurity density, are neglected in this approach. It is estimated that these corrections are still small for densities where only the lowest subband is occupied; see the Appendix in Ref. 3.

B. Impurity levels and impurity bands

We have seen that binding energies decrease with increasing wire radius. Clearly, for $R_0\rightarrow\infty$ one would expect to recover the energy levels of a three-dimensional hydrogen atom. However, this limit is not included in our approach, since the electron motion in the cross section of the wire is solely described by the envelope wave function for the confinement. Moreover, for the crossover to the three-dimensional hydrogen atom the energy distances between the subbands of the wire become very small, and all subbands must be taken into account.

However, from our notation of the states in the wire (subband, $n^{\pm}$) we can already identify the relation between the states in the quasi-one-dimensional and the three-dimensional hydrogen atoms. The impurity levels in the one-dimensional hydrogen atom transform into the impurity levels of the three-dimensional hydrogen atom when the wire radius becomes large: $R_0\rightarrow\infty$. From the symmetry and the degeneracy of the impurity levels in the quasi-one-dimensional system, this transformation can be studied, and the results are shown in Table II. Our classification is in agreement with earlier results given in Ref. 13, where the bound-state energies of the 1^+ and 2^- states of the first ($1s$ and $2p_z$) and second subbands ($2p_x$ and $3d_{xz}$) have been discussed.

In our numerical calculations within the multiple-scattering approach, we have only treated the impurity bands of the lowest subband. The Klauder approach can also be applied to the second subband since the electron-impurity interaction potential is available in analytical form.[10] From Fig. 1 it is already clear that the impurity levels for the second subband have a lower binding energy than the impurity levels for the first subband. Numerically we confirmed this fact in Figs. 3, 4, 6, and 7.

No experimental data for impurity levels in quasi-one-dimensional systems are available to date. However, we expect that such data will emerge soon, and our results presented in this paper should be useful in order to classify the states. In general, one can say that the binding energies in one-dimensional systems are much larger than in three- and two-dimensional systems.

C. Impurity band and band tail

With Fig. 10 we have estimated the critical density $N_{ic,n^{\pm}}$ for the merging of the impurity band with the con-

TABLE II. Notation for the wave functions of the hydrogen atom in the wire and in three dimensions.

Wire				Three dimensions
Subband	State	m	Degeneracy	
1	1^+	0	1	$1s$
1	2^-	0	1	$2p_z$
1	2^+	0	1	$2s$
1	3^-	0	1	$3p_z$
1	3^+	0	1	$3s$
1	4^-	0	1	$4p_z$
2	1^+	±1	2	$2p_x, 2p_y$
2	2^-	±1	2	$3d_{xz}, 3d_{yz}$
2	2^+	±1	2	$3p_x, 3p_y$
2	3^-	±1	2	$4d_{xz}, 4d_{yz}$
2	3^+	±1	2	$4p_x, 4p_y$
3	1^+	±2	2	$3d_{xx}, 3d_{yy}$
3	2^-	±2	2	$4d_{xxz}, 4d_{yyz}$
3	2^+	±2	2	$4d_{xzz}, 4d_{yzz}$
3	3^-	±2	2	$5d_{xxz}, 5d_{yyz}$
3	3^+	±2	2	$5d_{xzz}, 5d_{yzz}$
4	1^+	0	1	$3d_{zz}$
4	2^-	0	1	$4d_{xyz}$
4	2^+	0	1	$4d_{zz}$
4	3^-	0	1	$5d_{xyz}$

duction band. If the impurity band is completely filled, this density would correspond to the metal-insulator transition. However, we note that our theory for the Green function and the density of states cannot give full information for an Anderson transition which may occur in a partially filled band due to strong disorder. Moreover, the spin degeneracy of the impurity band is not considered in our approach. Therefore, the position of the Fermi energy in the weak screening limit was not discussed. In the strong screening limit we used a spin-degeneracy factor of 2 for the band tail in order to determine the Fermi energy.

Our estimation for $N_{ic,n}\pm$, as given in Eq. (17), corresponds to the merging of impurity and conduction bands. The numerical value should not be taken too seriously. However, our calculation indicates a transition from the impurity-band regime to the band-tail regime for quasi-one-dimensional systems with a finite concentration of *charged* impurities. Note that within a multiple-scattering approach applied to a δ-function random potential, such a calculation has already been done by Klauder[2] and more recently in much more detail in Ref. 36.

D. Band tail: single-particle relaxation time

In the Born approximation a simple relation can be derived between the single-particle relaxation time τ_s, determined by the self-energy as

$$1/\tau_s = \Sigma''(k=k_m,\varepsilon_F)/2 \ , \tag{19}$$

and the transport relaxation time τ_t, determined by the mobility (or the resistivity). k_m is the wave number for which $A(k,\varepsilon_F)$ exhibits a maximum. These two scattering times are not identical, because only backscattering (large-angle scattering) contributes to the resistance (determined by the transport relaxation time), while small-angle scattering and large-angle scattering contribute equally to the single-particle relaxation time. These have been studied in two-dimensional systems (for a review, see Ref. 46) and they give information about the kinds of disorder present in the system. In one-dimensional systems the ratio $\tau_t/\tau_s > 1$ has also been recently discussed.[35]

For $R_0 = a^*$, $R=0$, and $N = 1\times10^6$ cm^{-1} for GaAs wires, the ratio $\tau_t/\tau_s = 6$ was given.[35] For the mobility we derived $\mu = 5\times10^3$ cm^2/V s.[10] We conclude that $1/\tau_s = 21$ meV $= 3.7$ Ry*. From Fig. 15 in the fifth Klauder approximation, we obtain $1/\tau_s = \Sigma''(k=k_m,\varepsilon_F)/2 = 1.45$ Ry*, and we conclude that the Born approximation gives a rough estimate of disorder effects in quasi-one-dimensional systems. A similar overestimation was found for the single-particle relaxation time in two-dimensional systems by comparing the Born approximation with the self-consistent Born approximation.[46]

In Ref. 35 an analytical formula was derived for the DOS in the presence of disorder. Using Eq. (15a) in Ref. 35 for $\varepsilon_F^{(0)}\tau_s = 1.7$ ($\varepsilon_F^{(0)} = 2.4$ Ry*; $1/\tau_s = 1.45$ Ry*), we find $\rho(\varepsilon_F)/\rho^{(0)}(\varepsilon_F^{(0)}) = 0.967$. From Fig. 13 we find $\rho(\varepsilon_F)/\rho^{(0)}(\varepsilon_F^{(0)}) = 0.97$. This result confirms that the analytical results for the DOS, given in Ref. 35, can be used to estimate disorder effects.

VII. CONCLUSION

The wave functions of a single Coulomb impurity in a cylindrical quantum wire have been studied within a variational approach. Analytical results for the variational equation have been obtained and implemented numerically. The squared Fourier-transformed electron wave functions determine the spectral density of the particle. Within our variational approach we calculated the wave functions in k space, and found good agreement with a numerical calculation based on the fifth Klauder approximation. The general behavior of impurity levels for charged impurities in quasi-one-dimensional systems has been presented.

The ground-state impurity band and the excited-state impurity bands for a small impurity concentration, as well as the band-gap renormalization for a large impurity concentration for charged impurities located in the center of the wire, have been studied within a multiple-scattering approach. The width of the impurity bands and the band-tail formation were interpreted as the result of overlapping wave functions in a random medium of charged centers. The conduction-band edge is found to be strongly renormalized by disorder. We conclude that the effects of disorder for the electron states are large and possibly important for the interpretation of measurements.

We have presented a systematic study of disorder effects for quasi-one-dimensional structures. We expect

that our results are important for a better understanding of disorder effects in (artificial) semiconductor quantum wires[7,8] and also for (natural) organic one-dimensional conductors.[47,48] Both systems are presently studied with very great intensity in theory and experiments. Some of the results presented here have been briefly outlined in a recent paper.[49]

Finally, it is important to remember that information about the density of states can be obtained by capacitance measurements.[28] Recent experiments with quantum wires[50,51] were focused to determine the subband-energy distances. With present state-of-the-art technology it is still difficult to reach the quantum limit with only one subband occupied. However, we believe that capacitance measurements could be a very useful tool to determine the effects of disorder to the density of states.

ACKNOWLEDGMENTS

We thank J. Serre for discussions. The "Laboratoire de Physique des Solides (URA 74)" and the "Groupe de Physique des Solides (URA 17)" are "Laboratoires associés au Centre National de la Recherche Scientifique (CNRS)." We wish to thank the CNUSC (Montpellier, France) for allocating computational resources through a grant from "Ministère de l'Education Nationale" for a C3NI joint project.

[1]P. Van Mieghem, Rev. Mod. Phys. **64**, 755 (1992).
[2]J. R. Klauder, Ann. Phys. (N.Y.) **14**, 43 (1961).
[3]J. Serre and A. Ghazali, Phys. Rev. B **28**, 4704 (1983).
[4]A. Gold, J. Serre, and A. Ghazali, Phys. Rev. B **37**, 4589 (1988).
[5]J. Serre, A. Ghazali, and A. Gold, Phys. Rev. B **39**, 8499 (1989).
[6]A. Ghazali, A. Gold, and J. Serre, Phys. Rev. B **39**, 3400 (1989).
[7]C. W. J. Beenakker and H. van Houten, in *Solid State Physics,* edited by H. Ehrenreich and D. Turnbull (Academic, New York, 1991), Vol. 44, p. 1.
[8]W. Hansen, J. P. Kotthaus, and U. Merkt, in *Nanostructured Systems,* edited by A. K. Willardson, A. C. Peer, and E. R. Weber, Semiconductors and Semimetals Vol. 35 (Academic, New York, 1992), p. 279.
[9]S. Flügge and H. Marschall, *Rechenmethoden der Quantentheorie* (Springer, Berlin, 1965).
[10]A. Gold and A. Ghazali, Phys. Rev. B **41**, 7626 (1990).
[11]J. Lee and H. N. Spector, J. Appl. Phys. **54**, 3921 (1983).
[12]J. Lee and H. N. Spector, J. Vac. Sci. Technol. B **2**, 16 (1984).
[13]G. W. Bryant, Phys. Rev. B **29**, 6632 (1984).
[14]G. W. Bryant, Phys. Rev. B **31**, 7812 (1985).
[15]J. Lee and H. N. Spector, J. Appl. Phys. **57**, 366 (1985).
[16]J. A. Brum, Solid State Commun. **54**, 179 (1985).
[17]T. Kodoma and Y. Osaka, J. Phys. Soc. Jpn. **55**, 3941 (1986).
[18]F. A. P. Osorio, M. H. Degani, and O. Hipólito, Phys. Rev. B **37**, 1402 (1988).
[19]G. Weber, P. A. Schulz, and L. E. Oliveira, Phys. Rev. B **38**, 2179 (1988).
[20]J. A. Brum and G. Bastard, Superlatt. Microstruct. **4**, 443 (1988).
[21]B. Sukumar and K. Naveneethakrishnan, Solid State Commun. **74**, 295 (1990).
[22]N. P. Montenegro, J. López-Gondar, and L. E. Oliveira, Superlatt. Microstruct. **9**, 5 (1991).
[23]P. Csavinszky and H. Oyoko, Phys. Rev. B **43**, 9296 (1991).
[24]A. Ghazali and I. C. da Cunha Lima, Mod. Phys. Lett. B **6**, 587 (1992).
[25]A. Latgé, N. P. Montenegro, and L. E. Oliveira, Phys. Rev. B **45**, 9420 (1992).
[26]S. I. Tsonchev and P. L. Goodfriend, J. Phys. B **25**, 4685 (1992).
[27]D. S. Chuu, C. M. Hsiao, and W. H. Mei, Phys. Rev. B **46**, 3898 (1992).
[28]T. Ando, A. B. Fowler, and F. Stern, Rev. Mod. Phys. **54**, 437 (1982).
[29]F. A. P. Osório, M. H. Degani, and O. Hipólito, Phys. Rev. B **37**, 1402 (1988).
[30]E. A. De Andrada e Silva, I. C. da Cunha Lima, and A. Ferreira da Silva, Phys. Rev. B **37**, 8537 (1988).
[31]A. Ferreira da Silva, Phys. Rev. B **41**, 1684 (1990).
[32]M. Takeshima, Phys. Rev. B **33**, 7047 (1986).
[33]M. J. Kearney and P. M. Butcher, J. Phys. C **20**, 47 (1987).
[34]P. Vasilopoulos and F. M. Peeters, Phys. Rev. B **40**, 10079 (1989).
[35]A. Gold, Phys. Rev. B **46**, 2339 (1992).
[36]K. Nicolic and A. Mac Kinnon, Phys. Rev. B **47**, 6555 (1993).
[37]P. Soven, Phys. Rev. **156**, 809 (1967); D. W. Taylor, *ibid.* **156**, 1017 (1967). For a review, see B. Velicky, S. Kirkpatrick, and H. Ehrenreich, *ibid.* **175**, 747 (1968).
[38]A. Gold and A. Ghazali, Phys. Rev. B **41**, 8318 (1990).
[39]D. Pines and P. Nozières, *The Theory of Quantum Liquids* (Benjamin, New York, 1966), Vol. I.
[40]I. S. Gradshteyn and I. M. Ryzhik, *Table of Integrals, Series, and Products* (Academic, New York, 1980).
[41]A. Gold, A. Ghazali, and J. Serre, Semicond. Sci. Technol. **7**, 972 (1992).
[42]G. Bastard, Phys. Rev. B **24**, 4714 (1980).
[43]N. F. Mott, *Conduction in Non-Crystalline Materials* (Oxford University Press, Oxford, 1987).
[44]O. Hipólito and V. P. Campos, Phys. Rev. B **19**, 3083 (1979); J. A. Brum, G. Bastard, and C. Guillemot, *ibid.* **30**, 905 (1984).
[45]P. A. Lee and T. V. Ramakrishnan, Rev. Mod. Phys. **57**, 287 (1985).
[46]A. Gold, Phys. Rev. B **38**, 10798 (1988).
[47]B. Dardel, D. Malterre, M. Grioni, P. Weibel, Y. Baer, and F. Lévy, Phys. Rev. Lett. **67**, 3144 (1991).
[48]T. Ishiguro and K. Yamaji, in *Organic Superconductors,* edited by M. Cardona, P. Fulde, K. von Klitzing, and H.-J. Queisser, Springer Series in Solid-State Sciences Vol. 88 (Springer, Berlin, 1989).
[49]A. Ghazali, A. Gold, and J. Serre, Semicond. Sci. Technol. **8**, 1912 (1993).
[50]T. P. Smith III, H. Arnot, J. M. Hong, C. M. Knoedler, S. E. Laux, and H. Schmid, Phys. Rev. Lett. **59**, 2802 (1987); T. P. Smith III, Surf. Sci. **229**, 339 (1990).
[51]H. Drexler, W. Hansen, S. Manus, J. P. Kotthaus, M. Holland, and S. P. Beaumont, Phys. Rev. B **49**, 14074 (1994).